RM E57K26

RESEARCH MEMORANDUM

AERODYNAMIC AND INLET-FLOW-FIELD CHARACTERISTICS AT A FREE-STREAM MACH NUMBER OF 3.0 FOR AIRPLANES WITH CIRCULAR FUSELAGE CROSS SECTIONS AND FOR TWO ENGINE LOCATIONS

By Murray Dryer and Roger W. Luidens

Lewis Flight Propulsion Laboratory
Cleveland, Ohio

NATIONAL ADVISORY COMMITTEE FOR AERONAUTICS

WASHINGTON

March 18, 1958

NATIONAL ADVISORY COMMITTEE FOR AERONAUTICS

RESEARCH MEMORANDUM

AERODYNAMIC AND INLET-FLOW-FIELD CHARACTERISTICS AT A FREE-STREAM MACH NUMBER OF 3.0 FOR AIRPLANES WITH CIRCULAR FUSELAGE CROSS SECTIONS AND FOR TWO ENGINE LOCATIONS

By Murray Dryer and Roger W. Luidens

SUMMARY

An experimental investigation of several airplane configurations was performed at a Mach number of 3.0 in a continuous flow tunnel at the Lewis laboratory. The configurations, considered conventional, had circular fuselage cross sections and a sweptback wing. One design incorporated two nacelles; the other had two side inlets located under the wing. A concept of interference cuts on the fuselage was also investigated for both designs.

The experimental results indicated no effect of the interference cuts in improving a maximum lift-drag ratio of 5.6 for the basic wing-body combination. This ratio was reduced to 5.1 when nacelles were added but was unaffected for the side-inlet configuration. Beneficial results were obtained with the side-inlet configuration in that Mach number reductions were realized at the inlet face on the order of two-dimensional compression based on positive angles of attack.

INTRODUCTION

As flight Mach numbers increase, the airplane-performance rewards for integrating the powerplant with the airframe also increase as illustrated analytically in reference 1. A Lewis program for studying airframe-engine arrangements also includes experimental investigations of which the results of this report are a part. The emphasis in these experimental studies is on the engine installation and, in particular, on a study of the interactions between the engine and airframe with the object of determining favorable interference effects. The information presented in this report includes the external aerodynamics of the airframe also the effects of engine location and a survey of the flow field at the engine inlet.

The airplanes for this investigation were to represent initially manned interceptors of about 25,000 pounds gross weight, using hydrocarbon fuels, and designed for a Mach number of 3.5. This concept influenced the choice of wing shape and the ratio of fuselage to wing size. The powerplant was assumed to be a lightweight engine with a high airflow over the Mach number range and might be an air turborocket as described in reference 2 or a very low compressor-pressure-ratio turbojet. A lightweight engine permits powerplant location further from the center of gravity than is possible with a heavy engine.

The present tests were made at a nominal Mach number of 3.0 and at Reynolds numbers which varied from 3.6×10^6 to 9.9×10^6 based on body length.

SYMBOLS

The following symbols are used in this report:

A	axial force
b	span
C_D	drag coefficient, D/q_0S_w
$C_{D,o}$	drag coefficient at zero lift
C_L	lift coefficient, L/q_0S_w
C_{L_α}	lift curve slope measured at zero lift
C_m	pitching-moment coefficient, $\mathcal{M}/q_0S_w\bar{c}$
C_n	yawing-moment coefficient referred to 50-percent m.a.c., $\mathcal{N}/q_0S_wb$
C_Y	side-force coefficient, Y/q_0S_w
ΔC_A	increment in axial-force coefficient
$\Delta C_{A,fr}$	increment in axial-force coefficient due to internal-duct friction
$\Delta C_{F,e}$	incremental correction in axial-force coefficient due to inlet location
$\bar{c}/2$	referred to 50-percent m.a.c.
D	drag
d	hydraulic diameter, in.
F	thrust function, $pS(1 + \gamma M^2)$

f	local duct friction coefficient
$\bar{f}$	mean apparent duct friction coefficient
L	lift
L/D	lift-drag ratio
ΔL	engine length, in.
l	body length
M	Mach number
$\mathcal{M}$	pitching moment
m.a.c.	mean aerodynamic chord of wing
$\mathcal{N}$	yawing moment
p	static pressure, lb/sq in. abs
q	dynamic pressure, $\frac{\gamma}{2} pM^2$, lb/sq in. abs
r	local body radius
r_{max}	maximum body radius
S	area
S_{fr}	fuselage frontal area
S_w	wing area, including portion submerged in fuselage
t/c	wing thickness to chord ratio
x	body longitudinal coordinate
Y	side force
V	fuselage volume, cu in.
α	angle of attack, deg
β	angle of sideslip, deg
γ	ratio of specific heats, 1.4
ε	angular change of inlet flow due to airplane interference

λ angle of exhaust with respect to free-stream direction in plan view

Φ momentum, $\int_A (p - p_0)dS + \int_A \gamma p M^2 \, dS$

Subscripts:

e exit

fr friction

in inlet

max maximum

o zero lift

tu turning

w wing

0 free stream

Superscript:

* referred to Mach number of 1.0

APPARATUS

Wind Tunnel

The investigation was conducted in the Lewis laboratory 1- by 1-foot block tunnel at a nominal Mach number of 3.0. The tunnel-inlet total pressure can be varied between 10 and 54 pounds per square inch absolute. Tunnel-inlet total temperature was maintained near 100° F, and the specific humidity was maintained sufficiently low to make condensation effects negligible.

Model Support

The model was supported from a sting attached to a strut. The sting could be pivoted about the leading edge of the strut, and the strut could be translated into or out of the tunnel so that the model could be kept at the center of the tunnel at angles of attack up to 12°. The mechanism was arranged so that the model pitched in the horizontal plane.

the balance temperature. Since the angle-of-attack plane was horizontal, there were no tare loads due to model weight. Strain-gage readings were made with a self-balancing potentiometer.

Models

The models, shown in figures 1 and 2, had identical wing locations on the fuselage. The fore and aft thirds of the fuselage were determined by the equation for the Sears-Haack body:

$$\frac{r}{r_{max}} = \left(1 - \frac{x}{l/3}\right)^{3/2}$$

and the center third was cylindrical.

The basic fuselage shape was modified in an attempt to incorporate the favorable interference effects described in detail in reference 3. The interference cuts were bounded by Mach lines in a vertical plane from the wing leading edge or trailing edge. The angle of the interference plane was 3° to the vertical plane through the fuselage centerline. The fore interference cut was intended to generate a favorable lift interference on the wing. The aft interference cut was intended to generate a drag reduction on the fuselage. These cuts also effectively increased the fineness ratio of the fuselage fore- and afterbodies. The internal engine flow that would exist in a real airplane was simulated by constant area straight-through ducts having the correct external shape from a drag standpoint. The duct internal friction was subtracted from the model forces. The configurations were tested without tail surfaces.

Also shown on figures 1 and 2 are pertinent model areas and dimensions and a further explanation of the interference cuts on the fuselage. The full circular fuselage is not shown.

Instrumentation

Two types of runs - force and pressure - were made; the instrumentation differed for each type. The tunnel-inlet conditions of total temperature and pressure, test-section static pressure, and humidity were measured for all runs. For the force tests the instrumentation consisted of the strain gage, static-pressure measurements at the model base area, and static-pressure measurements in the internal flow at the engine exhaust.

For the pressure run the instrumentation consisted of rakes of pitot and static tubes located in the plane of the engine inlet.

PROCEDURE

Test Procedure

The following procedure was used for running the force tests. The installed strain-gage balance was calibrated in the wind tunnel. This procedure permitted calibration of the strut-sting strain-gage angular deflection as well as the primary and interaction characteristics of the strain gage as a function of the applied loads and moments. Before taking data, the tunnel was run to cool the model and strain gage to the steady-state operating temperature. The tunnel was then shut down but held at vacuum, and the potentiometer strain-gage readings were set at zero while the temperature remained constant. The tunnel was then restarted. Readings were taken at 2° increments at nominal angles of attack from 0° to $\pm 14^\circ$. At the lower angles of attack, the tunnel total pressure was maintained as high as the strain-gage-balance design loads permitted. As the angle of attack was increased, the tunnel pressure had to be decreased accordingly. This procedure resulted in lower free-stream Reynolds numbers at the higher angles of attack as indicated in all the figures.

The pressure runs were made at the same conditions as the force runs on an alternate sting which had no strain-gage installation.

Data Reduction

The true values of normal and axial force, moments, and angles of attack were determined from the calibrations and indicated readings. The corrections to be discussed later were then applied to the measured axial forces. The axial and the normal forces were then converted to lift and drag by the usual relations.

Base-pressure correction. - The axial force was corrected to that force which would have been measured had the base pressure been ambient.

Estimation of correction for engine internal friction force. - It was desired in the present studies to eliminate the engine internal friction force associated with the constant area, straight-through passages. A static- and total-pressure survey was made at the engine entrance, and a static pressure was measured at the engine exit. With this information it was possible to estimate the engine internal friction force using the method and information of references 4 and 5 and, in particular, table 4.26 of reference 4. This method assumes one-dimensional adiabatic frictional flow through a constant area duct.

The axial friction force coefficient on the inside of the duct is, using symbols of reference 5, as follows:

$$\Delta C_{A,fr} = \frac{A_{fr}}{\frac{\gamma}{2} p_0 M_0^2 S_w} = \frac{1}{\frac{\gamma}{2} p_0 M_0^2 S_w} (F_{in} - F_e) = \frac{F_{in}}{\frac{\gamma}{2} p_0 M_0^2 S_w} \left(1 - \frac{F_e/F^*}{F_{in}/F^*}\right) \tag{1}$$

where

$$\frac{F_{in}}{p_0 S_w} = \frac{p_{in}}{p_0} \frac{S_{in}}{S_w} (1 + \gamma M_{in}^2) \tag{2}$$

and M_0 is known. The terms p_{in}/p_0 and M_{in} were determined by rake measurements, and S_{in}/S_w was a known model characteristic. From M_{in} the parameters $(F/F^*)_{in}$ and $(p/p^*)_{in}$ were determined by reference 4.

The conditions at the exit were determined from

$$\left(\frac{p}{p^*}\right)_e = \left(\frac{p}{p^*}\right)_{in} \left(\frac{p_e}{p_0}\right) \left[\frac{1}{\left(\frac{p_{in}}{p_0}\right)}\right] \tag{3}$$

where (p_e/p_0) was determined experimentally from a rake.

As a correlating parameter, a mean apparent friction coefficient, defined as

$$\bar{f} = \frac{1}{L_{max}} \int_0^{L_{max}} f \, dx$$

may also be obtained (using ref. 4) from the expression

$$4\bar{f} \frac{\Delta L}{D} = \left(4\bar{f} \frac{L_{max}}{D}\right)_{in} - \left(4\bar{f} \frac{L_{max}}{D}\right)_e$$

where ΔL is the engine length.

For the model with nacelles, the static pressure at the engine exhaust could not be satisfactorily measured because of reflected shock waves from the inlet. In this case, the internal friction force was estimated using a mean apparent friction factor of 0.0018 that was chosen from the data for the side-inlet model. The tables of reference 4 were used in this case also.

Estimation of correction for engine internal flow turning. - A correction for engine internal flow turning is required in the circumstances shown in the following sketches:

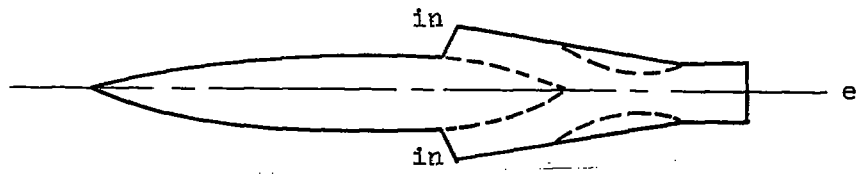

Schematic plan view of airplane

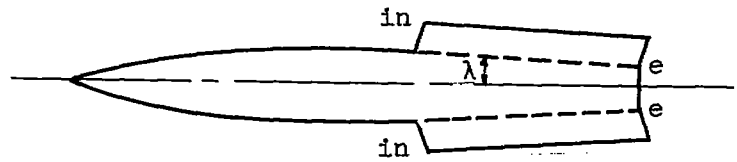

Schematic plan view of model

A correction must be made if, in the plan view of the airplane, the exhaust would be in the stream direction; but in the model the air taken in at the inlet was exhausted in a direction other than the stream direction. In the airplane, there is no axial force because of the turning or offset. The correction, approximately,

$$\Delta C_{A,tu} = \frac{\Phi_{in} - \Phi_e \cos \lambda}{q_0 S_w}$$

was generally very small.

Estimation of correction for engine-inlet momentum. - The conventional definition of thrust is as follows:

$$\Delta\Phi = \Phi_e - \Phi_0$$

where

$$\Phi = \int_S (p - p_0)dS + \int_S \gamma p M^2 dS$$

The conventional airplane drag must then be modified by an inlet-location force given by $F_e = \Phi_0 - \Phi_i \cos \varepsilon$ if the inlet were subjected to interference from the airframe. This concept was developed and evaluated in detail in reference 1. Such an inlet-location correction was applied to the present configurations to make comparisons between the configurations as equitable as possible (see following sketch).

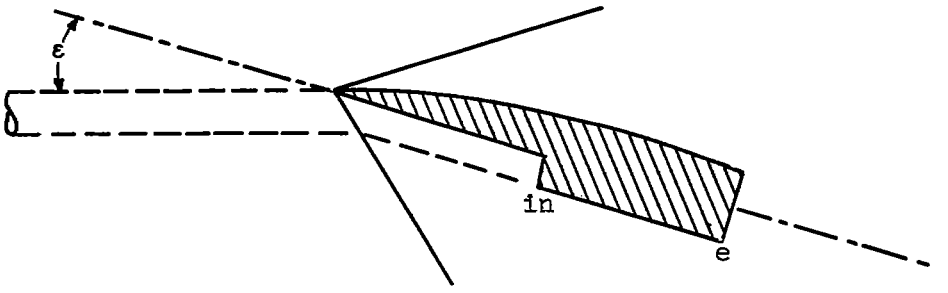

The correction was calculated as follows:

$$\Delta C_{F,e} = \frac{\Delta\Phi}{q_0 S_w} = \frac{\Phi_0 - \Phi_{in}\cos\varepsilon}{q_0 S_w} = 2\frac{p_{in}}{p_0}\frac{M_{in}}{M_0}\sqrt{\frac{1 + 0.2M_{in}^2}{1 + 0.2M_0^2}}\left(\frac{S_{in}}{S_w}\right)$$

$$\left[1 - \frac{M_{in}}{M_0}\sqrt{\frac{1 + 0.2M_0^2}{1 + 0.2M_{in}^2}}\cos\varepsilon - \frac{\cos\varepsilon}{\gamma M_{in} M_0}\sqrt{\frac{1 + 0.2M_0^2}{1 + 0.2M_{in}^2}}\left(1 - \frac{1}{p_{in}/p_0}\right)\right]$$

In this equation M_0 is known; p_{in}/p_0 and M_{in} are determined by rake measurements, and S_{in}/S_w is a known model characteristic.

In the case of the present models, this correction was also small.

The combined correction of "inlet-location force" and "engine-duct internal friction" is approximately equivalent to the calculated difference in momentum between the model-engine duct exit and the free stream.

RESULTS AND DISCUSSION

The results are presented as angle of attack, drag coefficient, and moment coefficient about the 50-percent-wing mean aerodynamic chord as a function of lift coefficient. Also presented are lift-drag ratios and local Mach numbers at the engine inlet as a function of angle of attack. Side-force and yawing-moment coefficients about the 50-percent-wing mean aerodynamic chord at zero angle of attack are presented as a function of angle of sideslip. These data are presented for the configuration with and without both the engines and fuselage interference cuts at a Mach number of 2.97. The results of all configurations are summarized in table I.

Configuration with Nacelles

No interference cuts. - Figure 3 presents the longitudinal aerodynamic characteristics of the body-wing configuration with the full round fuselage. Although the configuration had the wing mounted high on the fuselage, the lift-curve slope (fig. 3(a)) was essentially the same at plus and minus angles of attack, and the drag polar (fig. 3(b)) was essentially symmetrical. The lift-curve slope for the configuration based on wing area was 0.026 as compared with the two-dimensional flat plate value of 0.025. The slope of the pitching-moment curve (fig. 3(c)), although nonlinear, indicates that the neutral point was ahead of the 0.5 mean aerodynamic chord of the wing. Figure 3(d) presents the configuration lift-drag ratio. The maximum lift-drag ratio, about 5.6, was the same at plus and minus angles of attack.

Figure 4 presents the longitudinal aerodynamic characteristics for the configuration with nacelle engines. The lift at zero angle of attack, the lift-curve slope at positive angles of attack, and the level of the drag coefficient were increased because of the addition of the nacelles. The maximum lift-drag ratio decreased from 5.6 without nacelles to 5.1 and 5.2 at plus and minus angles of attack, respectively.

Figure 5 presents directional aerodynamic characteristics of the configuration with nacelles as a function of the sideslip angle. The configuration was directionally unstable about the 0.5 mean aerodynamic chord of the wing. By assuming a vertical tail with the same C_{Y_β} as the wing C_{l_α} and a tail moment arm of one wing span, a vertical tail area of 23 percent of the wing area would be required to produce neutral directional stability. The drag of the vertical tail obviously would reduce the lift-drag ratios shown in figure 3(d).

With interference cuts. - Figure 6 presents the longitudinal aerodynamic characteristics of the same body-wing combination previously discussed but with body interference cuts. The test results show that the interference cuts adversely affected the lift-curve slope, drag at zero lift, and the lift-drag ratio.

Figure 7 presents the longitudinal characteristics of the body-wing-engine combination with interference cuts. The effect of the cuts was to reduce the magnitude of the maximum lift-drag ratio from 5.1 to 5.0 at positive angles of attack and from 5.2 to 4.9 at negative angles of attack.

Configuration with Side Inlets

No interference cuts. - It may be considered that the body-wing combination of the previous models is also the body-wing combination for the

configuration with side inlets. The longitudinal characteristics of the configuration with side inlets, then, are presented in figure 8. A comparison of figure 3 with figure 8 shows that the maximum lift-drag ratio was essentially unaffected by the addition of the engines, inasmuch as both $C_{D,o}$ and C_{L_α} were increased.

With interference cuts. - Figure 9 presents the longitudinal characteristics of the side-inlet configuration with interference cuts on the fore part of the fuselage. The maximum lift-drag ratio was again about 5.6 and occurred at about a 4.6° angle of attack; however, at negative angles the maximum lift-drag ratio decreased from 5.5 to 5.3. In a comparison of the configuration with side inlets and the nacelle configuration, the placing of the engines in the fuselage will reduce the available storage volume.

Figure 10 presents the Mach numbers at the engine inlet. At zero angle of attack the average Mach number at the engine inlet was at free stream although the Mach number at the bottom of the inlet was about 0.14 lower than at the top. The bottom of the inlet felt the compression from the wing leading edge while the top of the inlet was influenced by the wing profile which produced some expansion. This local Mach number variation held for all the angles of attack investigated. At a 4.4° angle of attack, which was about the condition of maximum lift-drag ratio, the average Mach number ahead of the inlet was about 0.17 below free stream. The reduction in Mach number for two-dimensional flow (due to angle of attack alone) at a 4.4° angle of attack was 0.15. The remaining figures show that the Mach number at the inlet decreased for further increases in angle of attack and increased as expected at negative angles of attack.

Figure 11 presents the directional characteristics of the configuration with side inlets at zero angle of attack. Although also unstable about the wing 0.5 m.a.c., this configuration was less unstable than the configuration with nacelles (fig. 5).

SUMMARY OF RESULTS

The results indicated by the Mach 3.0 experimental conclusions are summarized as follows:

1. The highest lift-drag ratio in the present tests was 5.6 for a configuration with side inlets.

2. Interference cuts on the fuselage of the present design were ineffective in improving the configuration maximum lift-drag ratio.

3. The addition of nacelles at approximately one-half of the wing semispan reduced the maximum lift-drag ratio of the configuration without interference cuts from 5.6 to 5.1.

4. Mach number reductions on the order of two-dimensional values were obtained at the inlets of the side-inlet configuration.

Lewis Flight Propulsion Laboratory
National Advisory Committee for Aeronautics
Cleveland, Ohio, December 3, 1957

REFERENCES

1. Luidens, Roger W.: Arrangements of Jet Engine and Airframe for Increased Range. NACA RM E56L04, 1957.

2. Luidens, Roger W., and Weber, Richard J.: An Analysis of Air-Turborocket Engine Performance Including Effects of Component Changes. NACA RM E55H04a, 1956.

3. Ferri, Antonio, Clarke, Joseph H., and Casaccio, Anthony: Drag Reduction in Lifting Systems by Advantageous Use of Interference. PIBAL Rep. 272, Dept. Aero. Eng. and Appl. Mech., Polytech. Inst. Brooklyn, May 1955. (Contact AF-18(600)-694.)

4. The Johns Hopkins University Applied Physics Laboratory, ed.: The Mechanism and Thermodynamics of Steady One-Dimensional Gas Flow. NAVORD Rep. 1488, Vol. I of Handbook of Supersonic Aerodynamics, sec. 4, Dept. Navy, Bur. Ord., Apr. 1, 1950, pp. 4.1-4.155.

5. Shapiro, Ascher H.: The Dynamics and Thermodynamics of Compressible Fluid Flow. Vol. I. The Ronald Press Co., 1953.

TABLE I. - SUMMARY OF LONGITUDINAL AND DIRECTIONAL CHARACTERISTICS

[Free-stream Mach number, 3.0]

Number	Configuration	Angle of attack direction	Longitudinal									Directional		Reference
			$\left(\frac{L}{D}\right)_{max}$	α_{opt}, deg	C_{D_0}	α_0, deg	C_{L_α}	$\frac{dC_D}{dC_L^2}$	$C_{m_{a.c.}}$	$\left(\frac{dC_m}{dC_L}\right)_0$	(M_{in}) at $\left(\frac{L}{D}\right)_{max}$	C_{n_β}	C_{Y_β}	
1	Body - wing; without interference cuts	+	5.6	5.0	0.011	-0.2	0.026	0.71	-0.0023	0.091	----	--------	--------	Fig. 3
		-	5.6	-5.0			0.026				----			
2	Body - wing - Nacelles; without interference cuts	+	5.1	5.0	0.015	-0.6	0.029	0.62	-0.0074	0.080	2.97	-0.0052	-0.0061	Figs. 4 and 5
		-	5.2	-6.4			0.029				2.95			
3	Body - wing; with interference cuts	+	5.4	5.0	0.012	-0.4	0.024	0.77	-0.0023	0.115	----	--------	--------	Fig. 6
		-	5.1	-5.5			0.026				----			
4	Body - wing - Nacelles; with interference cuts	+	5.0	4.6	0.016	-1.0	0.028	0.63	-0.0057	0.086	2.96	--------	--------	Fig. 7
		-	4.9	-6.6			0.028				2.96			
5	Body - wing - Side inlets; without interference cuts	+	5.6	5.0	0.012	-0.4	0.028	0.65	-0.0052	0.023	----	--------	--------	Fig. 8
		-	5.5	-5.0			0.028				----			
6	Body - wing - Side inlets; with interference cuts	+	5.6	4.6	0.012	-0.5	0.028	0.70	0	-0.020	2.82	-0.0027	-0.0044	Figs. 9 to 11
		-	5.3	-5.4			0.028			0.023	3.33			

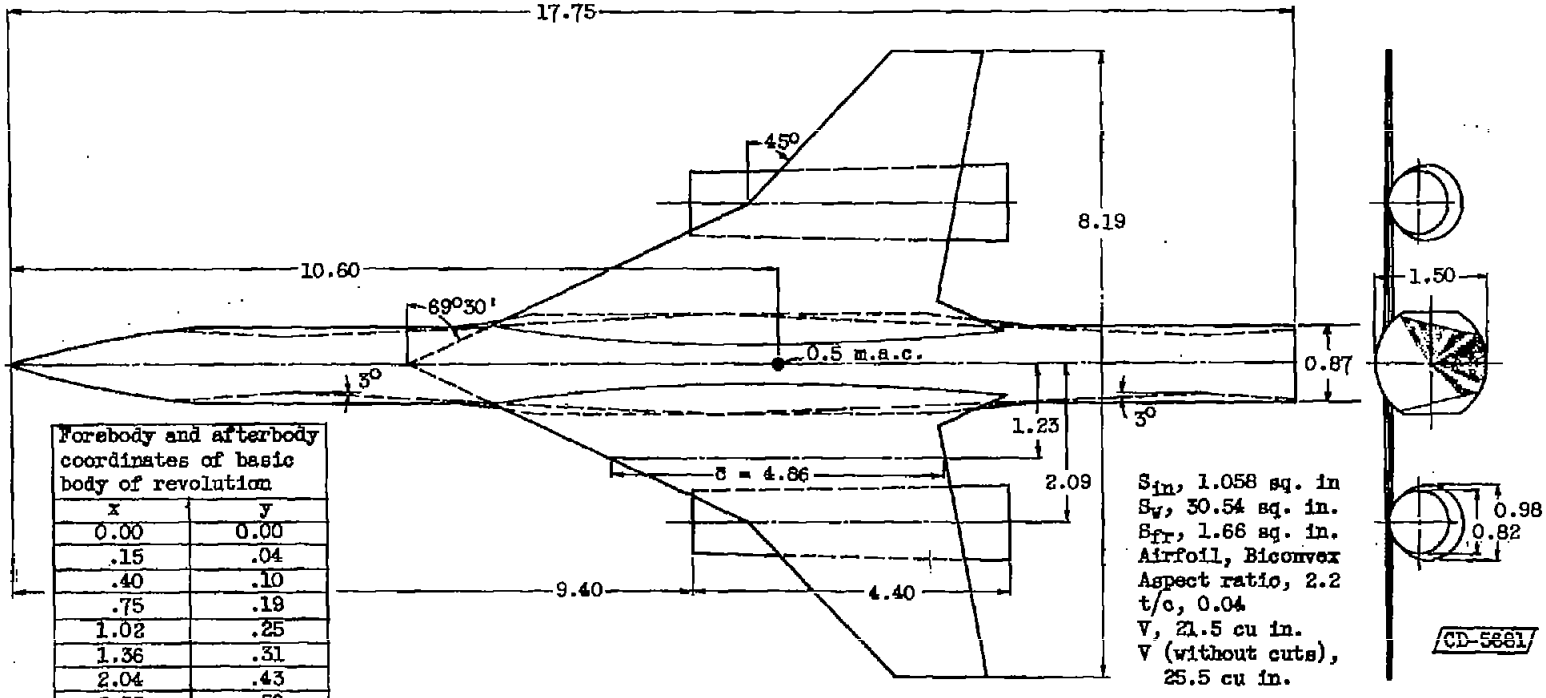

Forebody and afterbody coordinates of basic body of revolution

x	y
0.00	0.00
.15	.04
.40	.10
.75	.19
1.02	.25
1.36	.31
2.04	.43
2.53	.50
3.90	.65
5.26	.72
6.62	.75
9.93	.75

Figure 1. - Configuration with near circular fuselage and nacelles. (Configuration is shown with interference cuts. Alternate configuration has fuselage with full body of revolution.) (All dimensions in inches.)

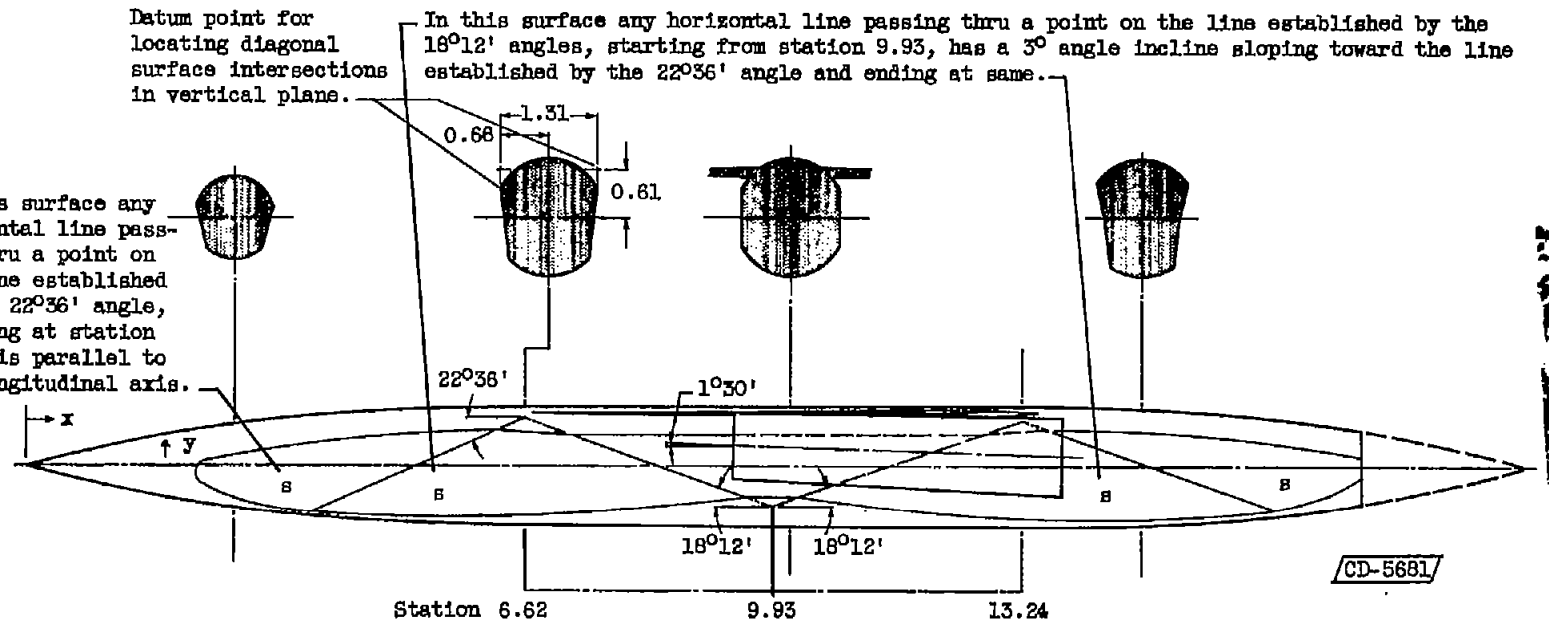

Figure 1. - Concluded. Configuration with near circular fuselage and nacelles. (Configuration is shown with interference cuts. Alternate configuration has fuselage with full body of revolution.) (All dimensions in inches.)

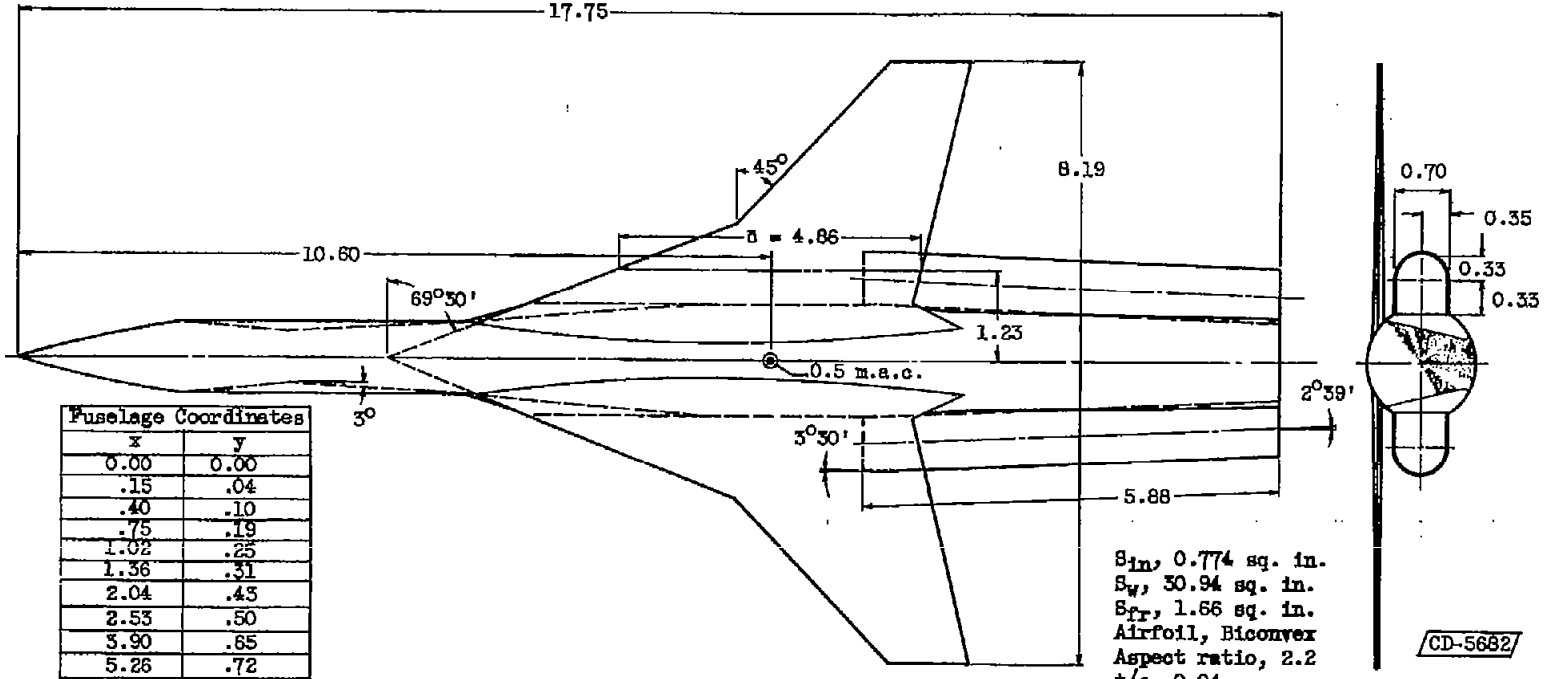

Fuselage Coordinates	
x	y
0.00	0.00
.15	.04
.40	.10
.75	.19
1.02	.25
1.36	.31
2.04	.43
2.53	.50
3.90	.65
5.26	.72
6.62	.75
Straight ↓ 17.75	Taper ↓ 0.68

Figure 2. - Configuration with near circular fuselage and side inlets. (Configuration is shown with interference cuts. Alternate configuration has only flats on sides of fuselage.) (All dimensions in inches.)

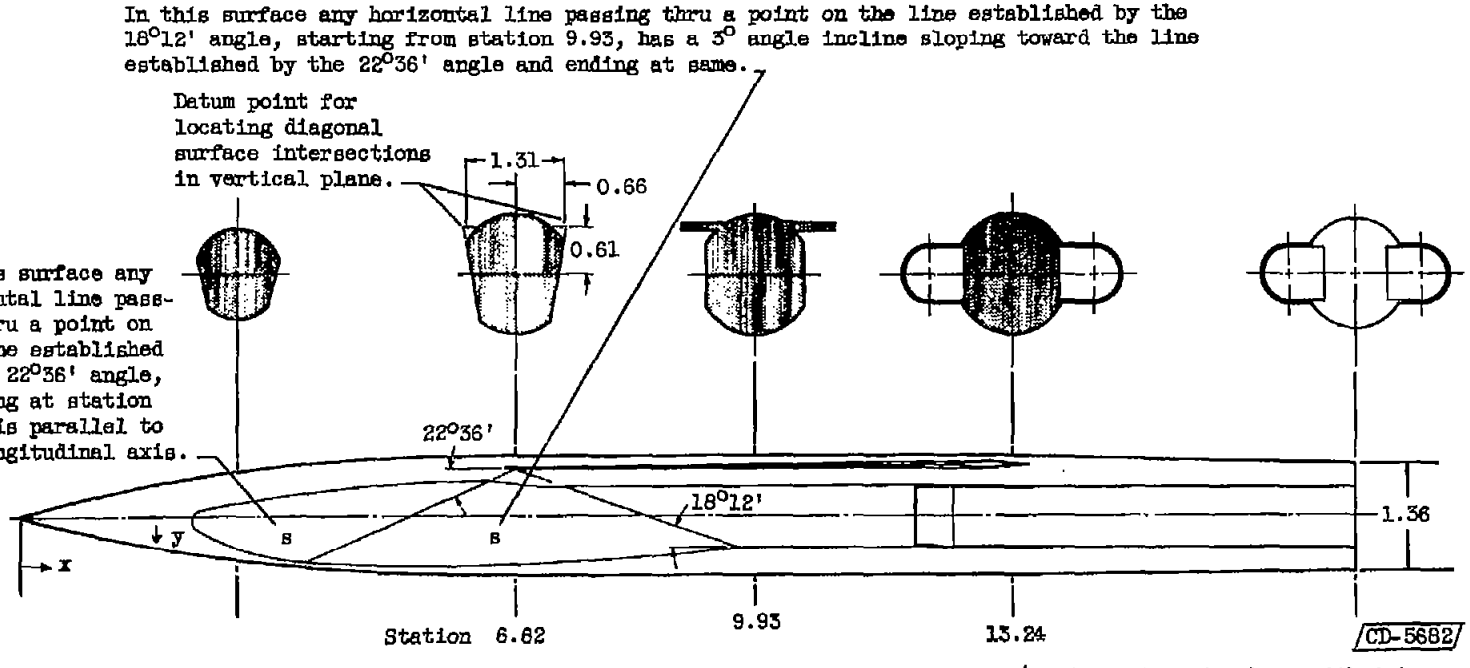

Figure 2. - Concluded. Configuration with near circular fuselage and side inlets. (Configuration is shown with interference cuts. Alternate configuration has only flats on sides of fuselage.) (All dimensions in inches.)

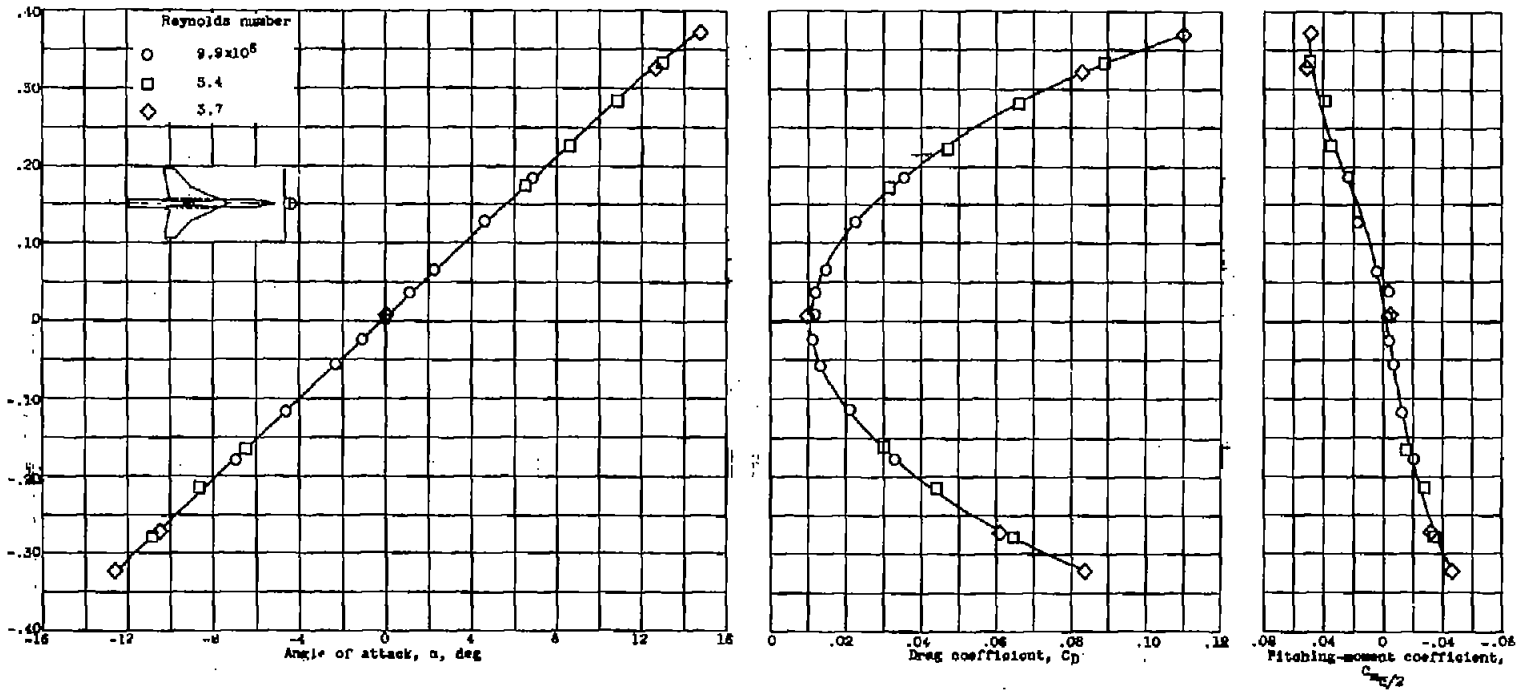

Figure 3. - Longitudinal aerodynamic characteristics of body-wing combination; without interference cuts. Free-stream Mach number, 3.0.

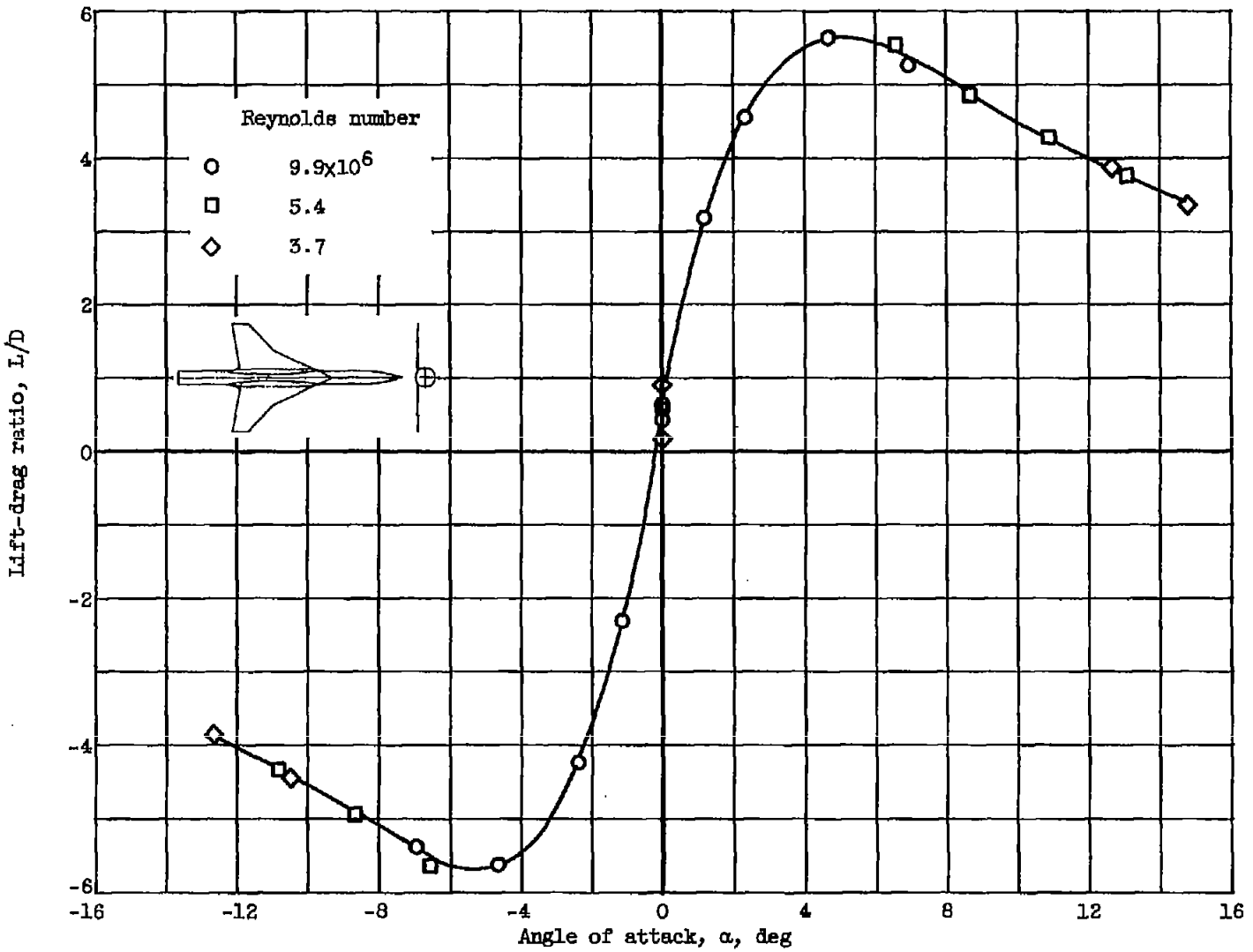

Figure 3. - Concluded. Longitudinal aerodynamic characteristics of body-wing combination; without interference cuts. Free-stream Mach number, 3.0.

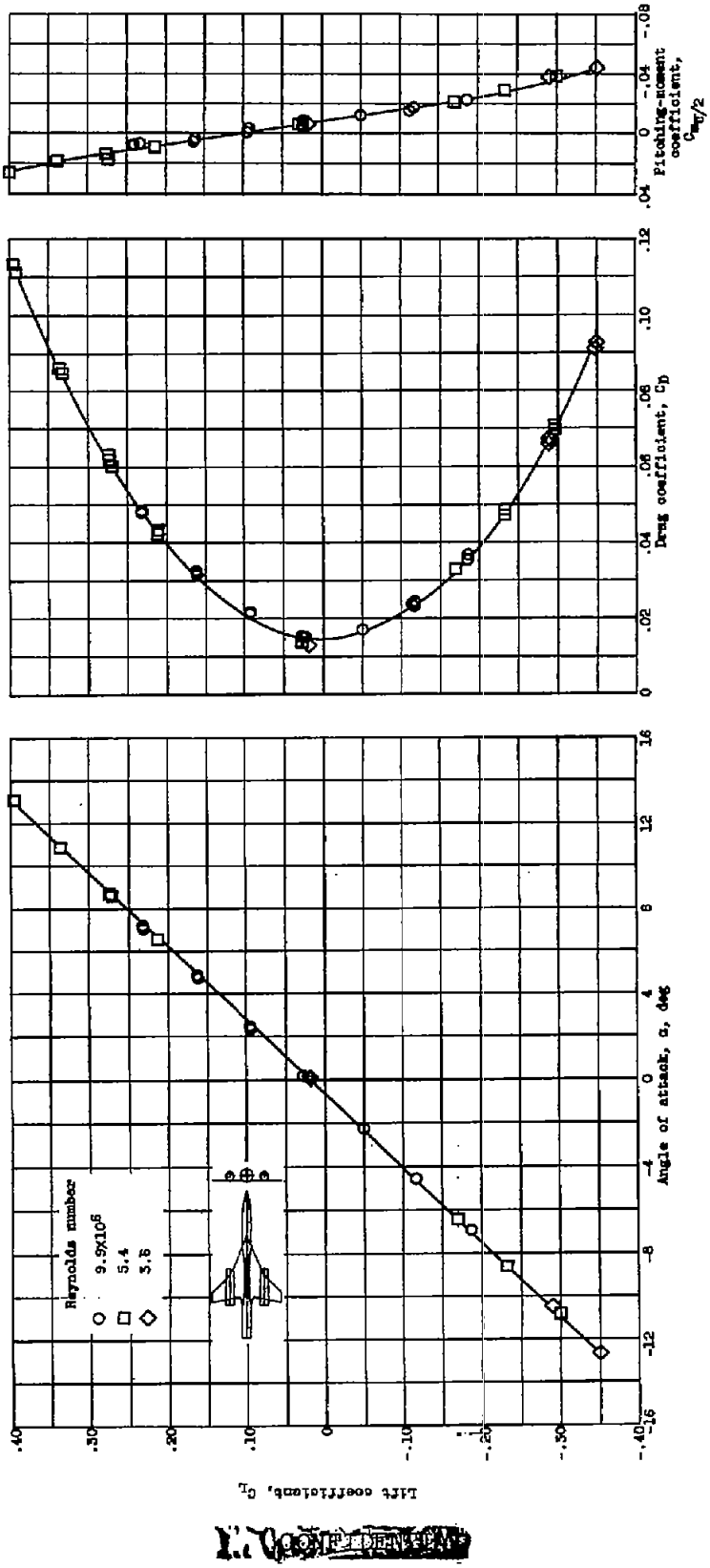

Figure 4. - Longitudinal aerodynamic characteristics of configuration with nacelles; without interference cuts. Free-stream Mach number, 3.0.

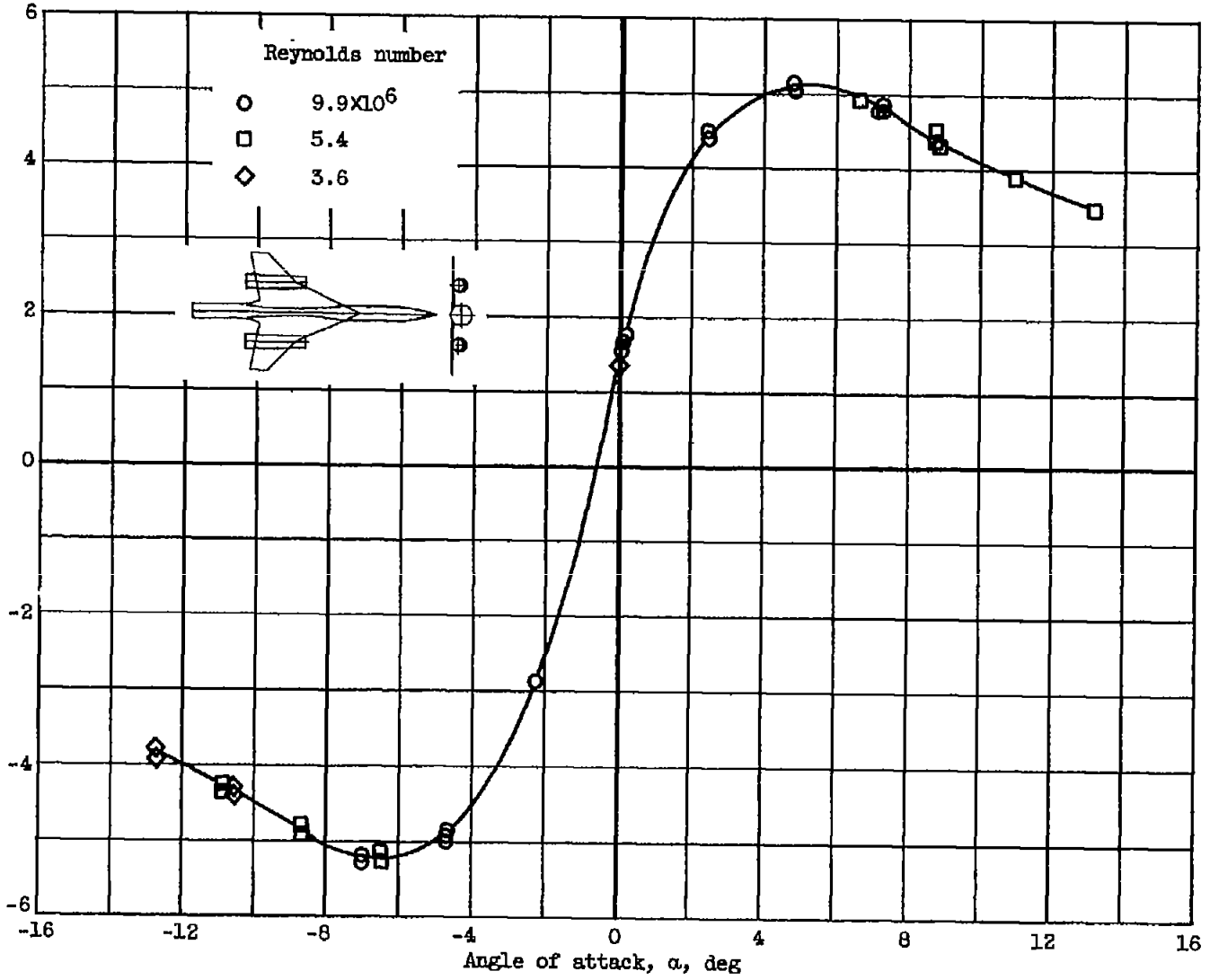

Figure 4. - Concluded. Longitudinal aerodynamic characteristics of configuration with nacelles; without interference cuts. Free-stream Mach number, 3.0.

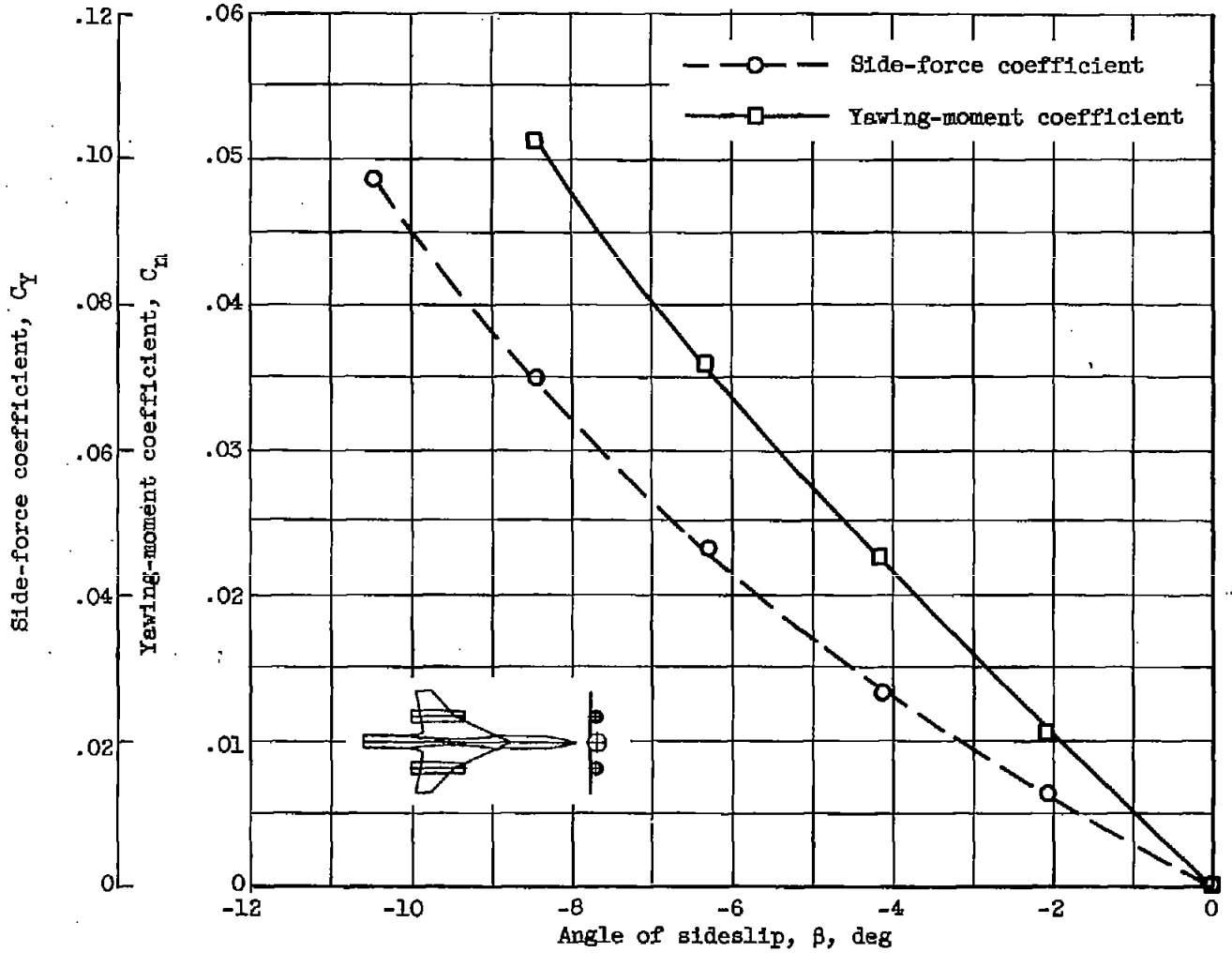

Figure 5. - Directional aerodynamic characteristics of configuration with nacelles; without interference cuts. Free-stream Mach number, 3.0; Reynolds number, 9.9×10^6.

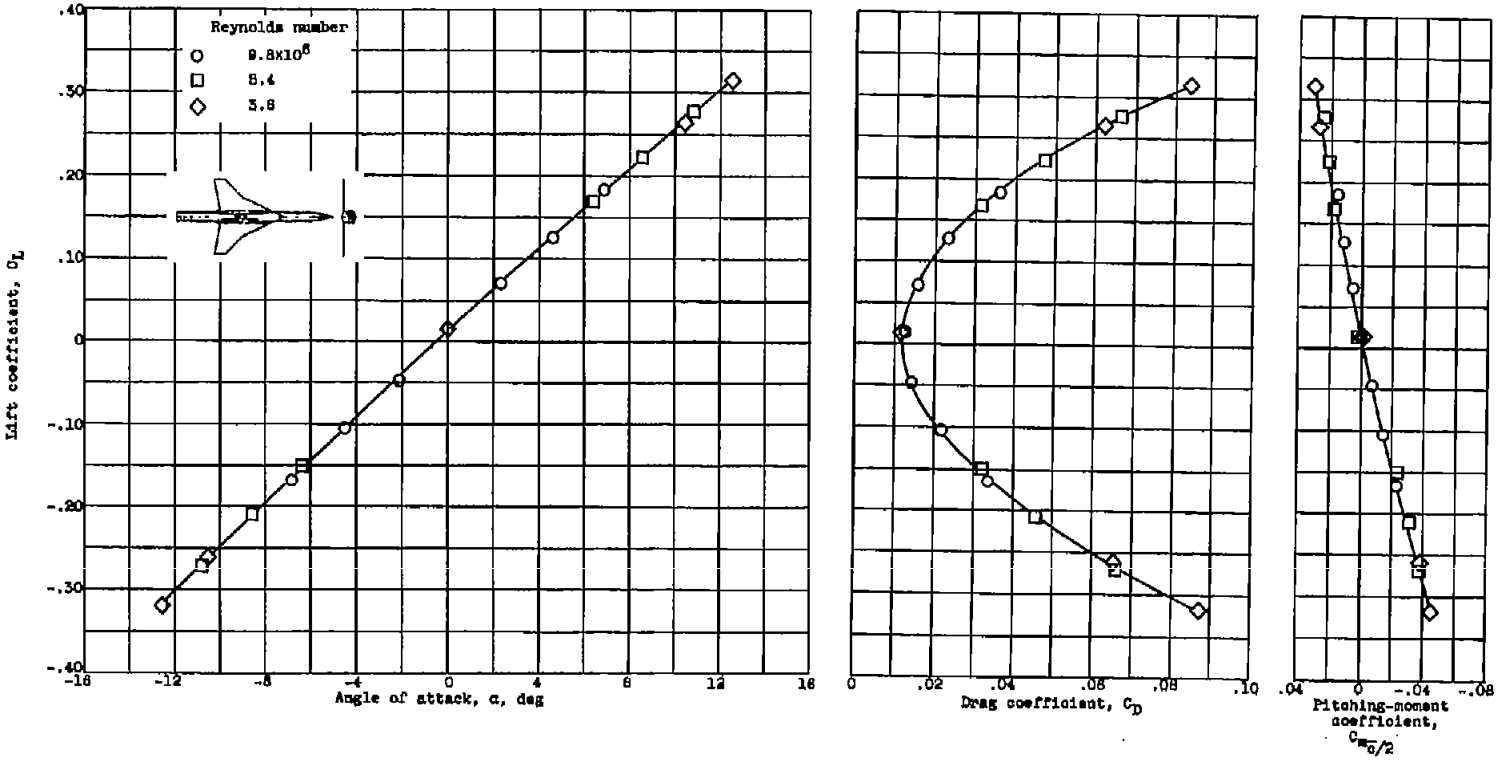

Figure 6. - Longitudinal aerodynamic characteristics of body-wing combination; with interference cuts. Free-stream Mach number, 3.0.

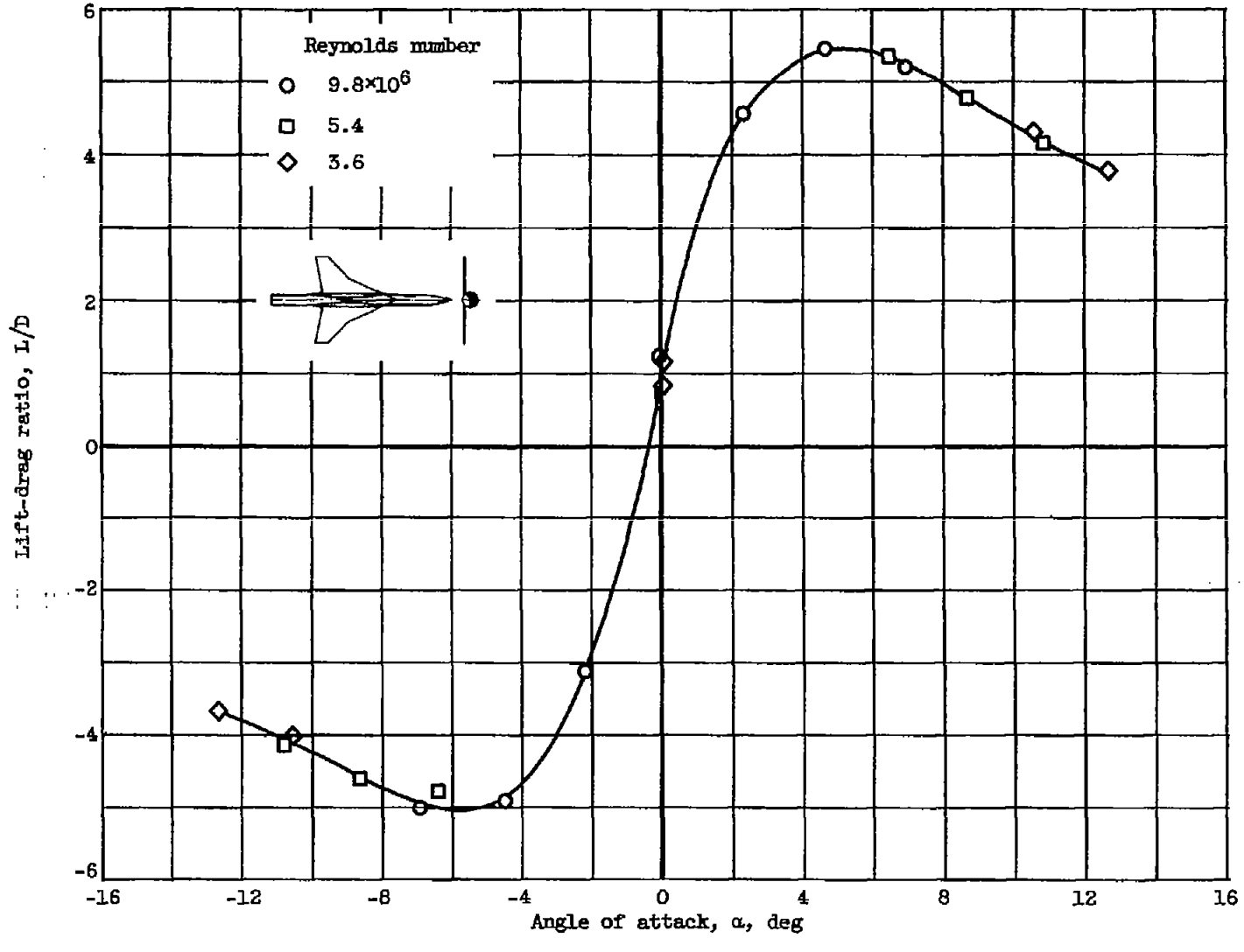

Figure 6. - Concluded. Longitudinal aerodynamic characteristics of body-wing combination; with interference cuts. Free-stream Mach number, 3.0.

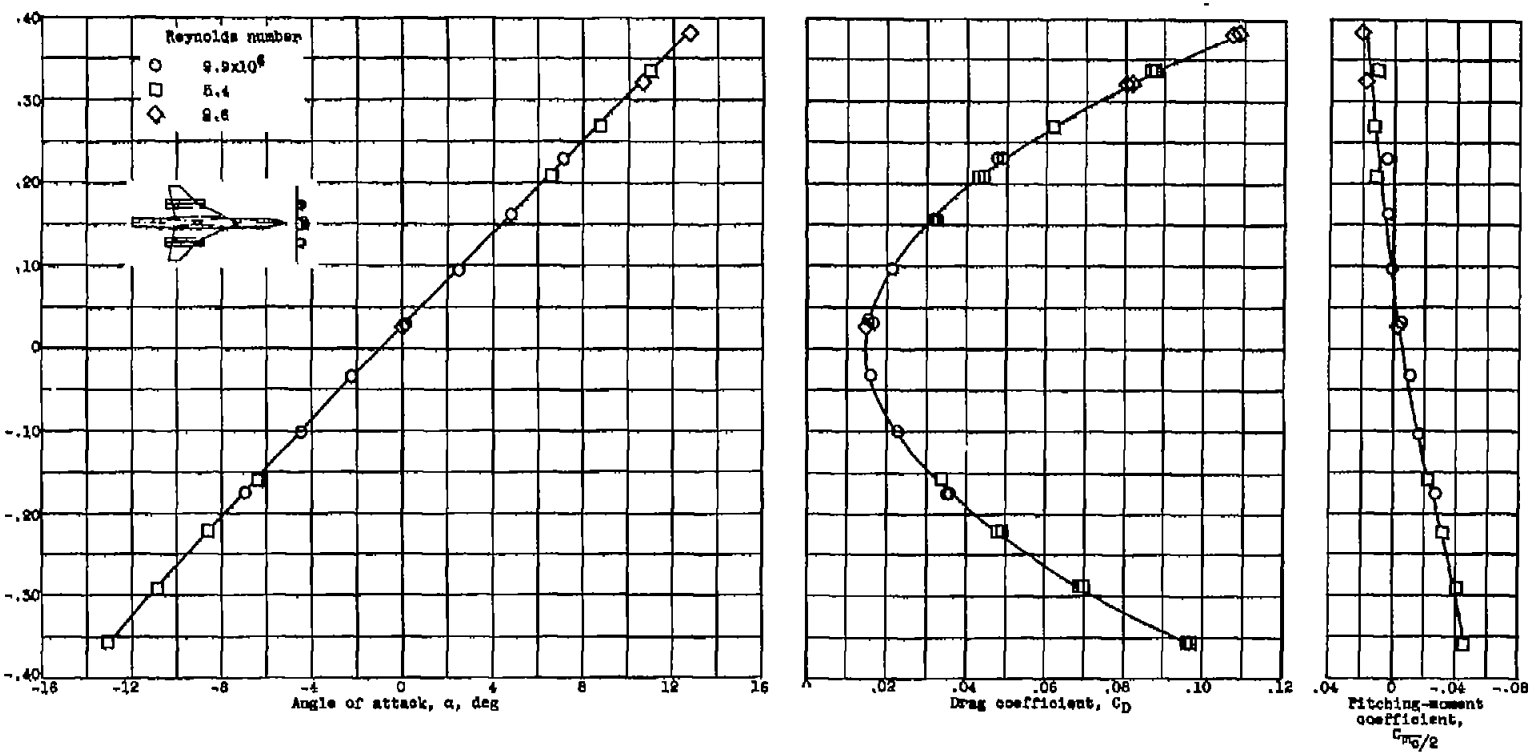

Figure 7. - Longitudinal aerodynamic characteristics of configuration with nacelles; with interference cuts. Free-stream Mach number, 3.0.

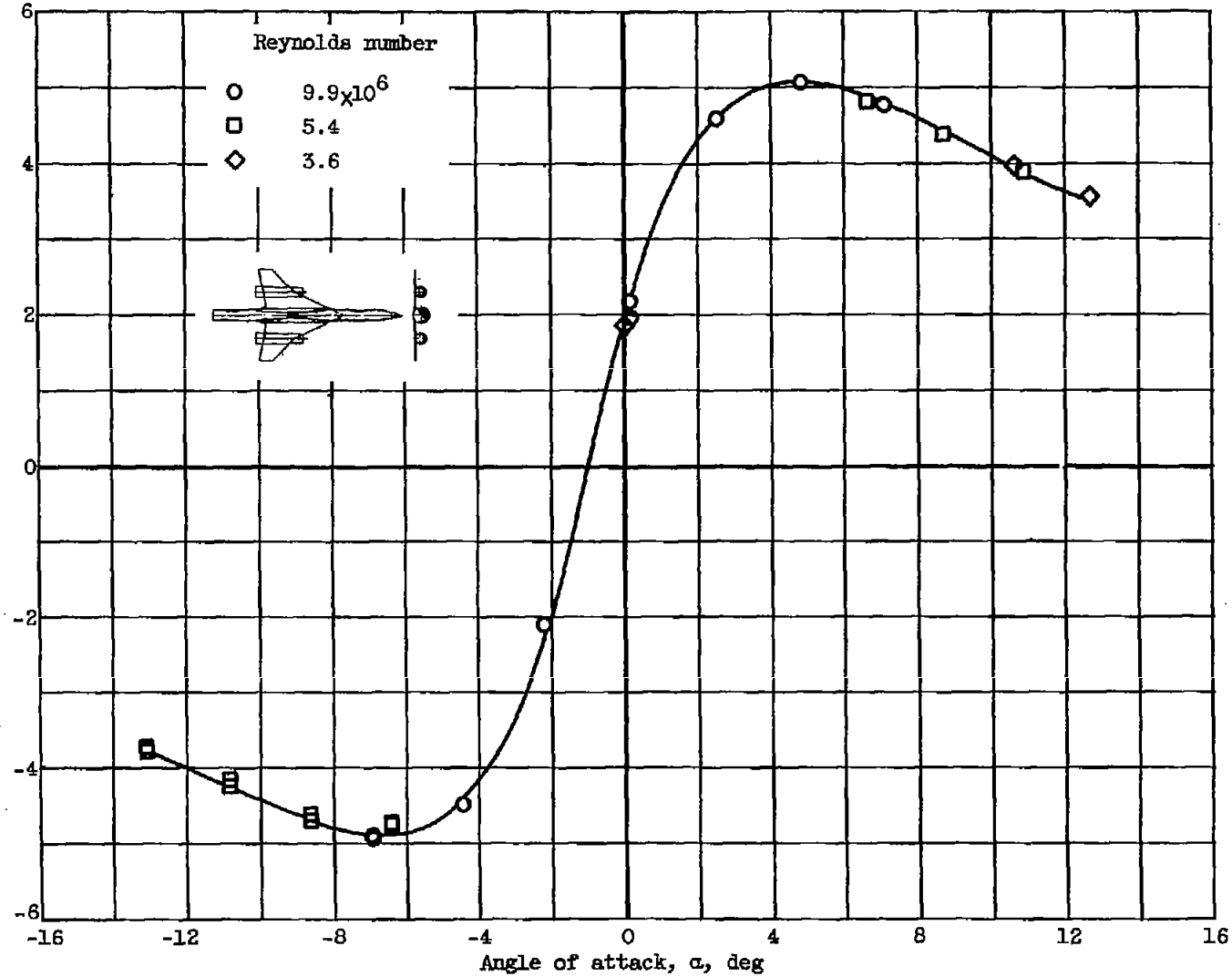

Figure 7. - Concluded. Longitudinal aerodynamic characteristics of configuration with nacelles; with interference cuts. Free-stream Mach number, 3.0.

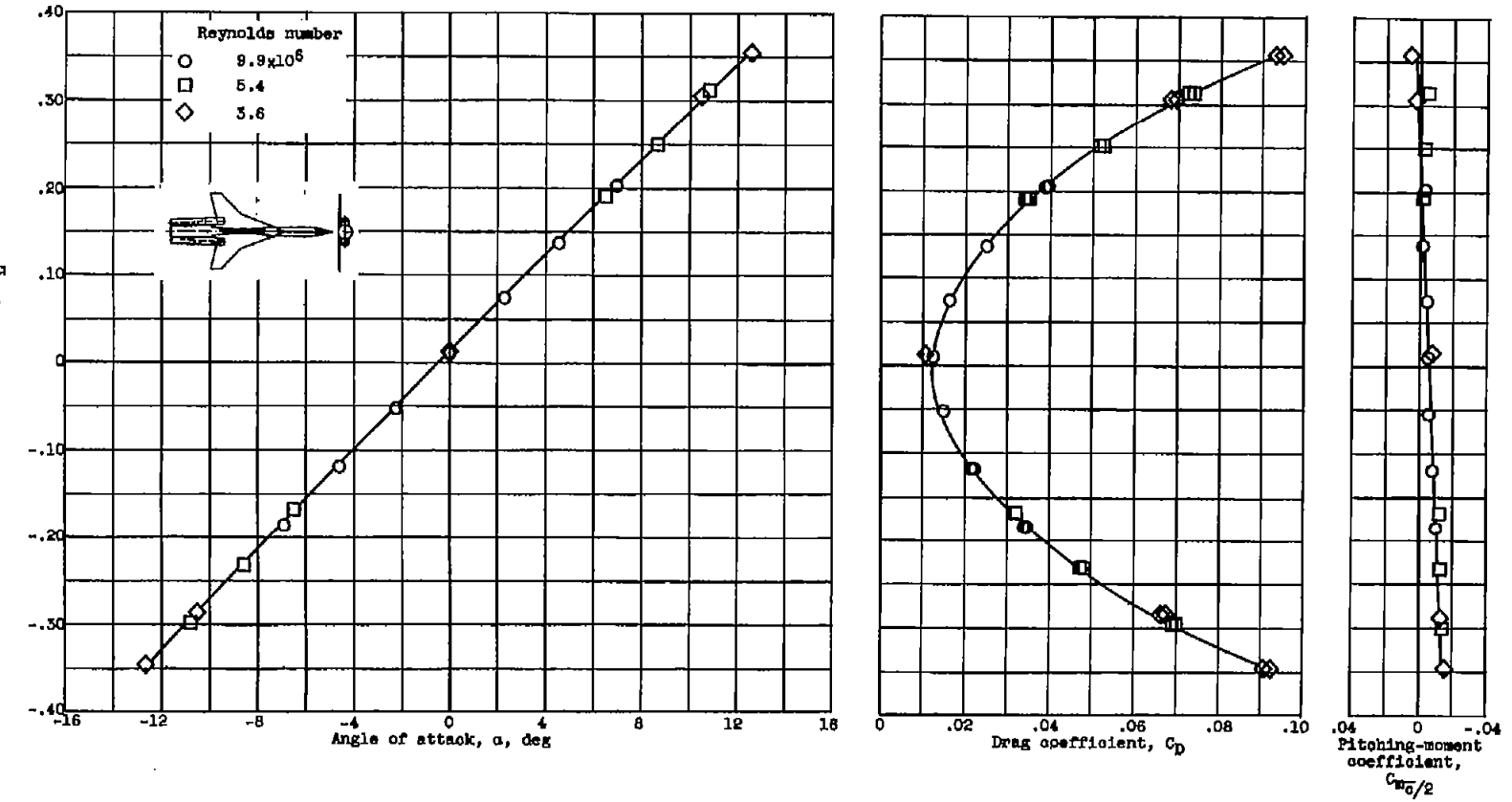

Figure 8. - Longitudinal aerodynamic characteristics of configuration with side inlets; without interference cuts. Free-stream Mach number, 3.0.

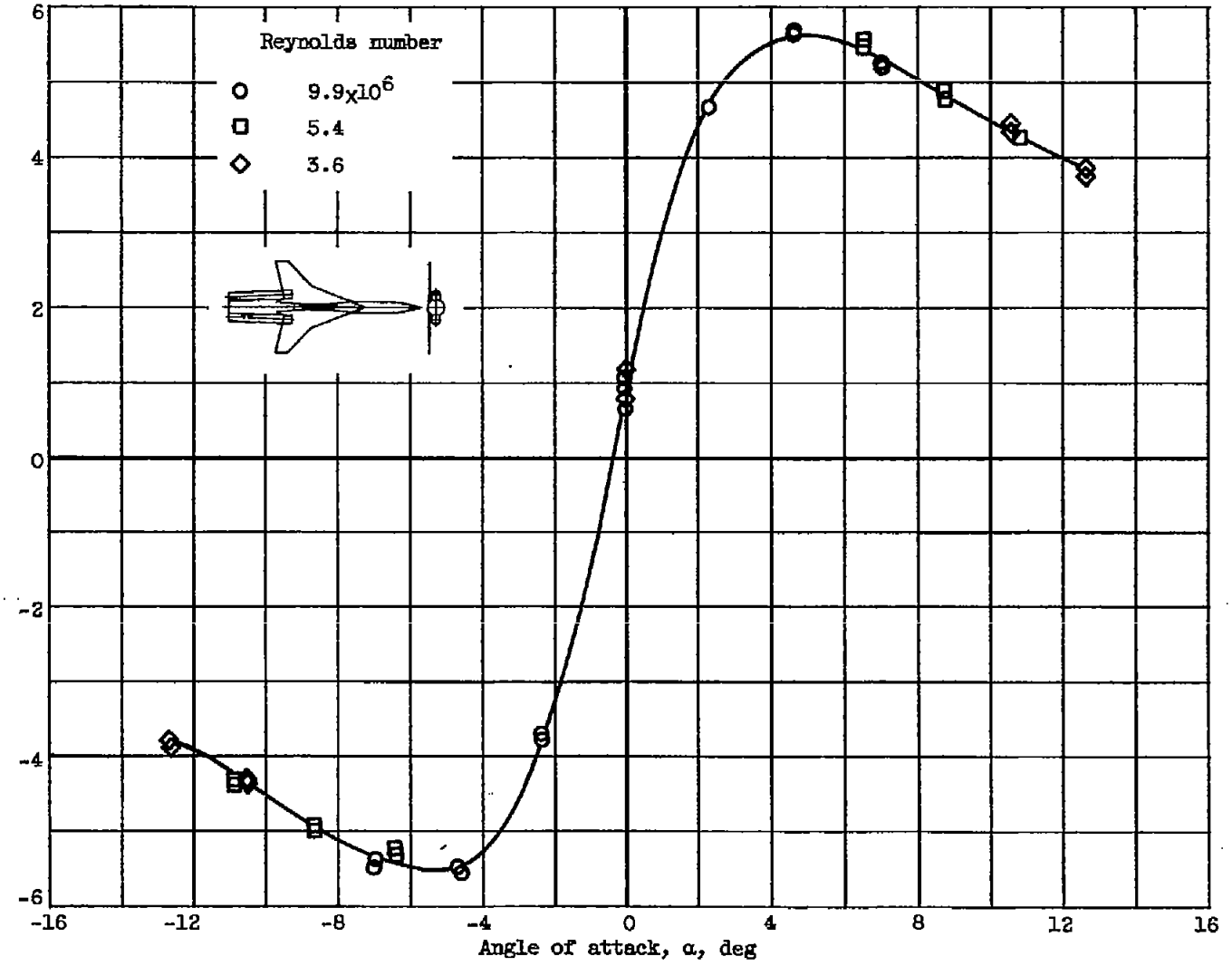

Figure 8. - Concluded. Longitudinal aerodynamic characteristics of configuration with side inlets; without interference cuts. Free-stream Mach number, 3.0.

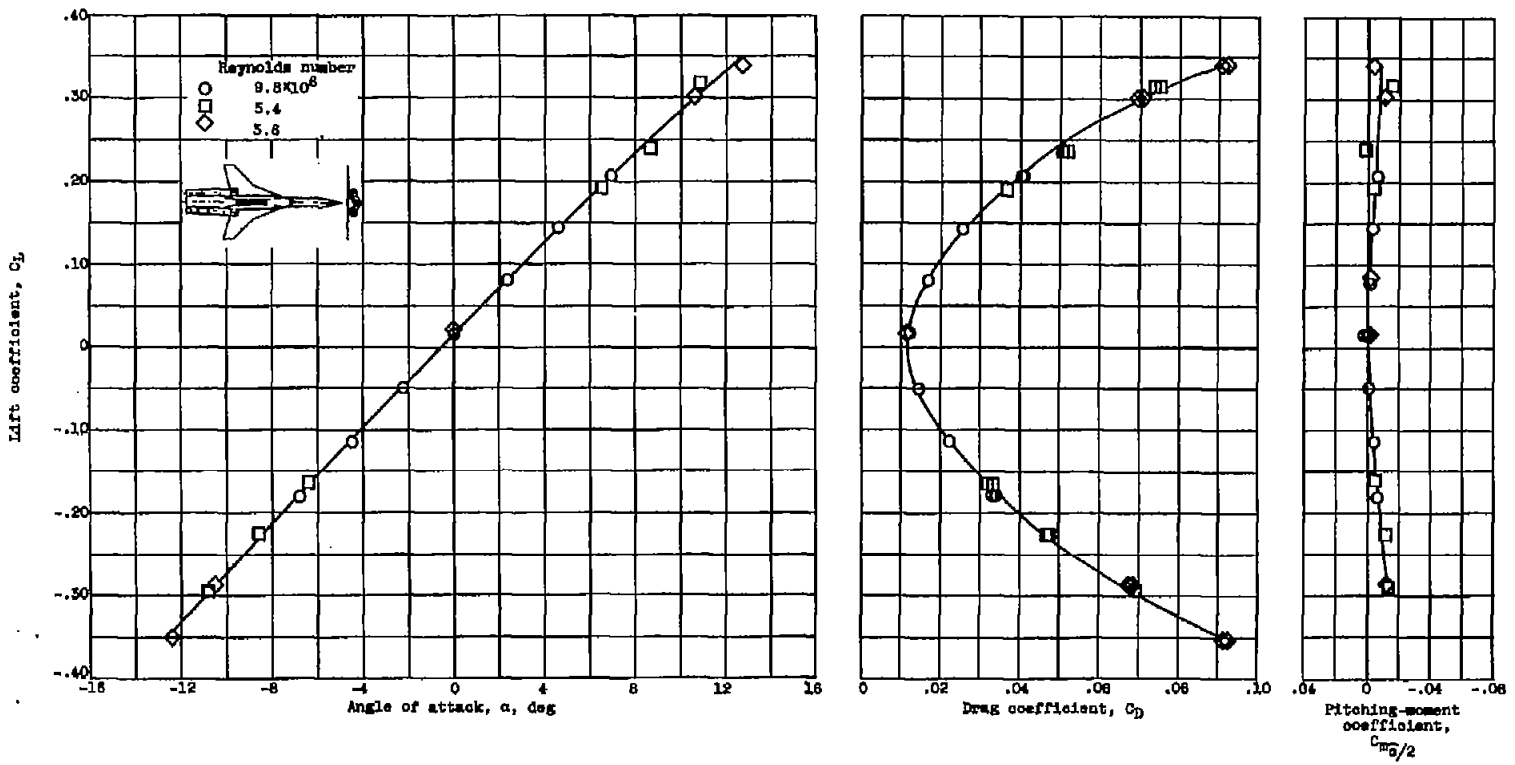

Figure 9. - Longitudinal aerodynamic characteristics of configuration with side inlets; with interference cuts. Free-stream Mach number, 3.0.

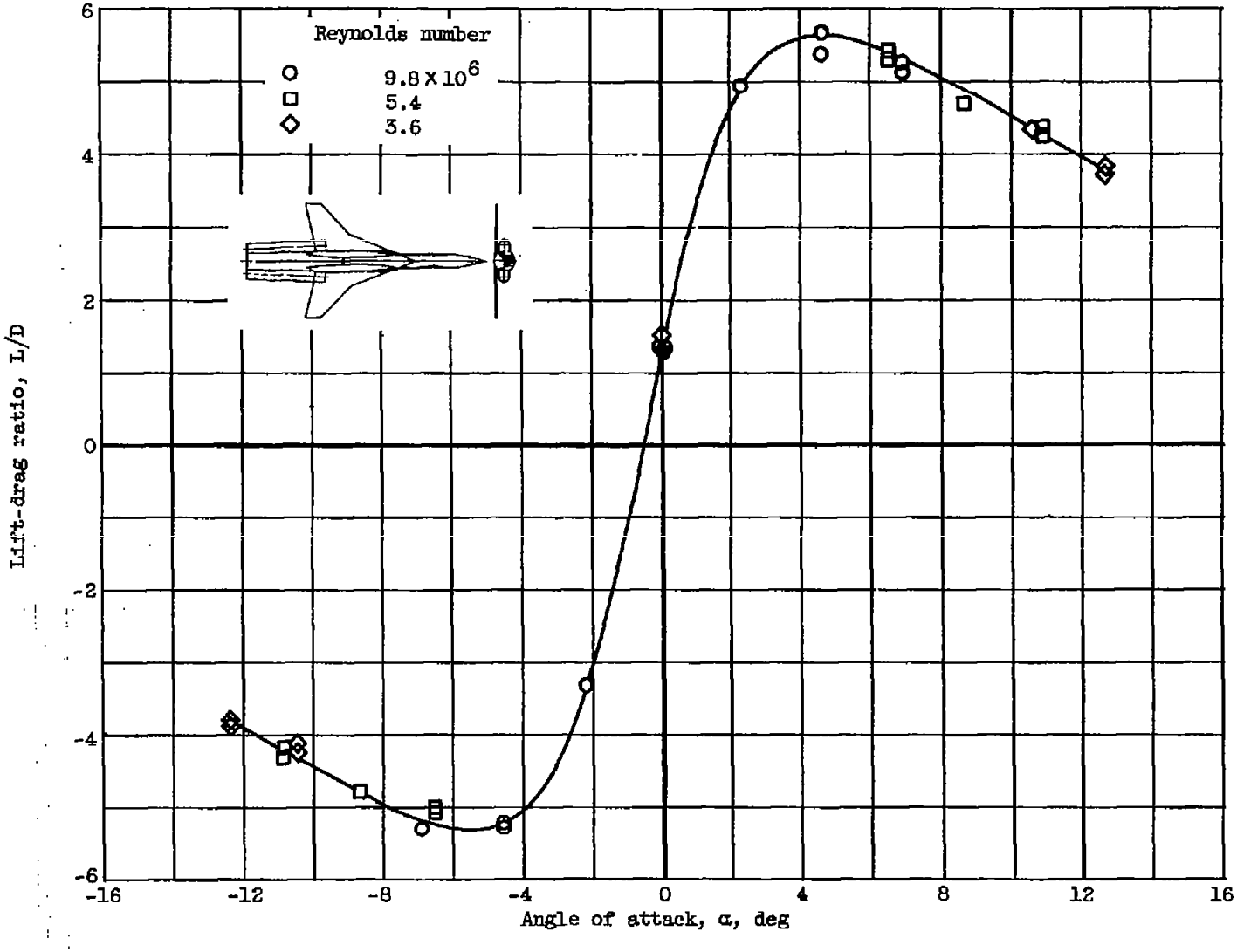

Figure 9. - Concluded. Longitudinal aerodynamic characteristics of configuration with side inlets; with interference cuts. Free-stream Mach number, 3.0.

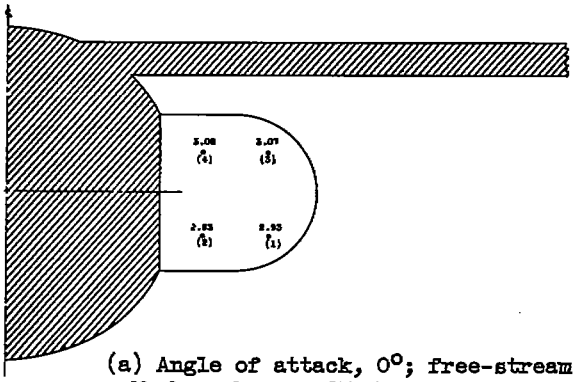

(a) Angle of attack, 0°; free-stream Mach number, 2.97; Reynolds number, 9.9×10^6.

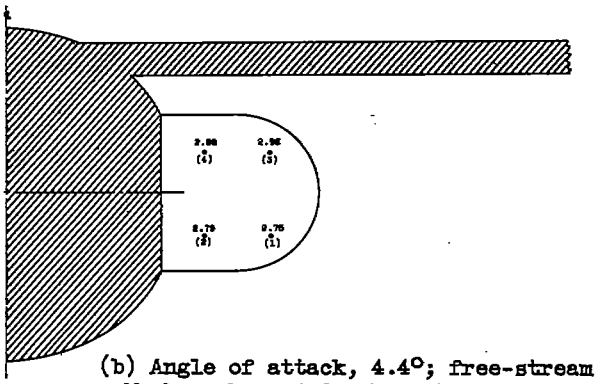

(b) Angle of attack, 4.4°; free-stream Mach number, 2.97; Reynolds number, 9.8×10^6.

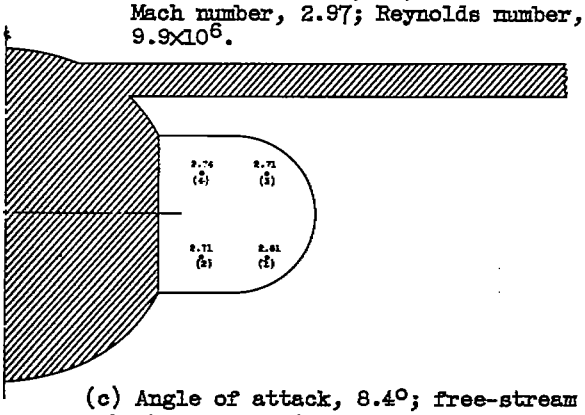

(c) Angle of attack, 8.4°; free-stream Mach number 2.96; Reynolds number, 5.4×10^6.

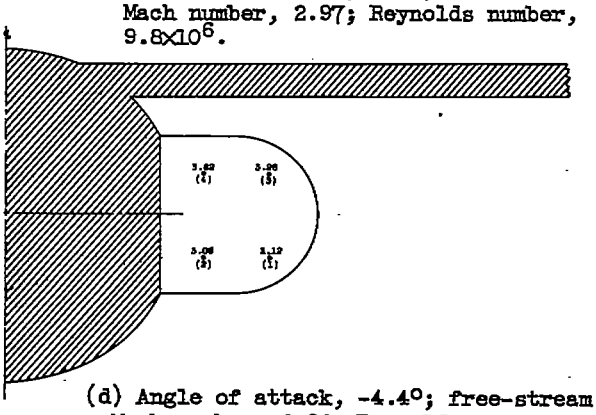

(d) Angle of attack, -4.4°; free-stream Mach number, 2.96; Reynolds number, 9.9×10^6.

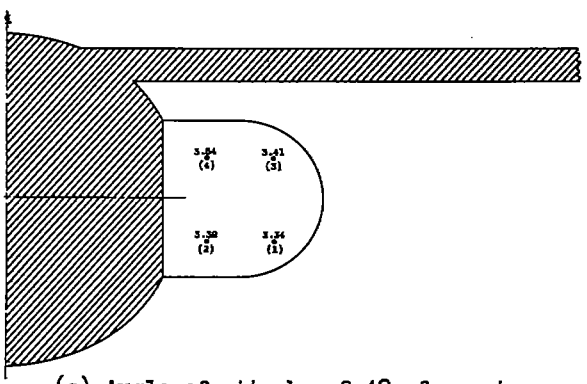

(e) Angle of attack, -8.4°; free-stream Mach number, 2.96; Reynolds number, 5.4×10^6.

Figure 10. - Mach-number distributions at engine inlet of side-inlet configuration with interference cuts and D-shaped engines.

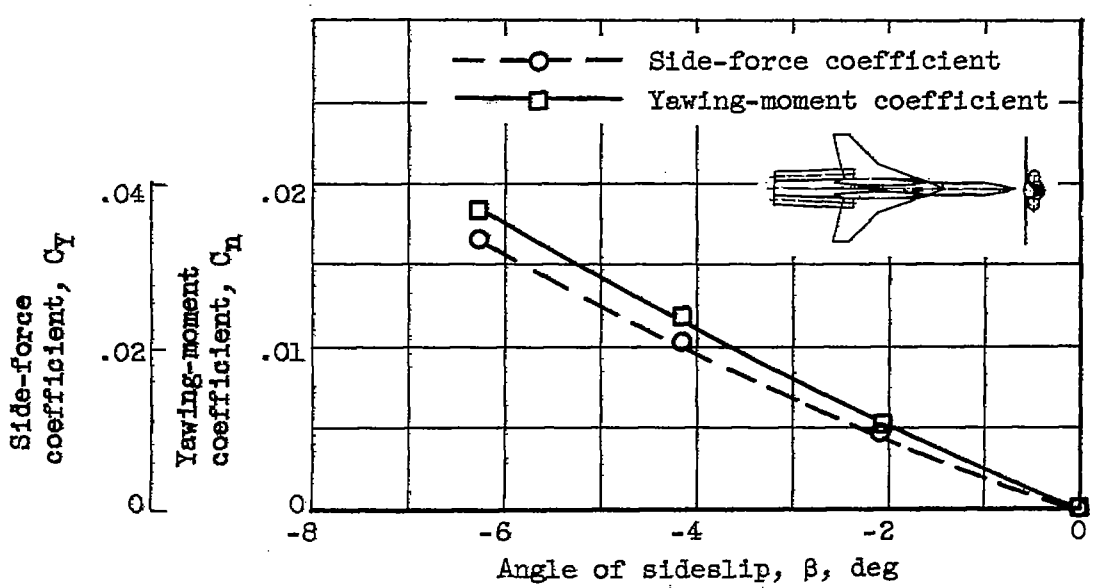

Figure 11. - Directional aerodynamic characteristics of configuration with side inlets and interference cuts. Mach number, 3.0; Reynolds number, 9.6×10^6.

NACA - Langley Field, Va.